Efficacy of high-frequency, low-voltage plasma immersion ion implantation of a bar-shaped target

Xiubo Tian, Zhaoming Zeng, Xuchu Zeng, Baoyin Tang, and Paul K. Chu[a]
Department of Physics and Materials Science, City University of Hong Kong, 83 Tat Chee Avenue, Kowloon, Hong Kong

(Received 6 December 1999; accepted for publication 24 May 2000)

Elevated-temperature plasma immersion ion implantation (PIII) increases the surface hardness and thickness of the modified layer and is traditionally performed at a high energy (typically above 5 keV) and low current density. In this article, we report the benefits of a different approach by high-frequency, low-voltage plasma immersion ion implantation (HLPIII). Experiments and a two-dimensional theoretical simulation are conducted to demonstrate the advantages of the process on a bar-shaped sample in terms of ion dose, dose uniformity, and modified layer thickness. Simulation of the sheath dynamics illustrates that the thinner plasma sheath in HLPIII is geometrically more conformal to the target surface, and the incident ion flux is more uniform along the exposed surface when compared to the traditional high-voltage PIII process. The higher ion dose and thicker modified layer can be attributed to the higher ion current density. HLPIII is thus the preferred technique to enhance the surface properties of large and complex-shaped specimens such as a metal track. © *2000 American Institute of Physics.* [S0021-8979(00)02717-1]

I. INTRODUCTION

Plasma immersion ion implantation (PIII) circumvents the line-of-sight limitation of conventional ion implantation and obviates the need for complicated target manipulation and beam rastering for the implantation of objects possessing a complex geometry.[1–4] However, for tribological applications, PIII suffers from two shortcomings. The first one is the large lateral dose variation that depends on the process parameters.[5–7] The other one is the thin modified layer that is generally less than 100 nm thick for low temperature PIII[8,9] thereby yielding unsatisfactory results when a heavy load is exerted on the treated surface in the field. The alternative is to conduct a PIII process at an elevated temperature or high voltage to increase the thickness of the modified layer, but a high temperature may cause undesirable structural and phase changes in the materials whereas a high voltage may degrade the ion dose uniformity on nonplanar samples. In this work, we report the use of high-frequency, low-voltage plasma immersion ion implantation (HLPIII)[10–12] on a bar-shaped sample resembling a track used as a transportation mechanism in a machine. Similar to a railroad track, both the top and upper half of the side surfaces are in contact with moving parts and premature failure can occur requiring enhancement of the surface properties. Experiments and theoretical simulation are performed to investigate the benefits and mechanism of HLPIII in terms of the ion dose, ion flux uniformity, and modified layer thickness using such a bar-shaped sample.

II. EXPERIMENT

To demonstrate HLPIII into a nonplanar track-shaped specimen, we performed our experiments on a stainless steel bar 300 mm long, 30 mm wide, and 30 mm high. As shown in Fig. 1, it was laid on top of a copper target platen 150 mm in diameter and 6 mm thick. Small pieces of stainless steel (Fe-60 at. %, Cr-27 at. %, Ni-8 at. %, and C-2.5 at. %) were affixed to the bar at three locations, on top (position 1), and on the side (positions 2 and 3). They were detached from the bar after the PIII experiments and analyzed by sputtering Auger electron spectroscopy to disclose the elemental depth profiles. The PIII experiments were performed using the multifunction PIII instrument at the City University of Hong Kong.[13] To demonstrate the effectiveness of the low voltage process, implantation was carried out at 2 and 15 kV. A custom made IGBT-based modulator[14] and a hard tube base pulsing modulator[13] were used for the low-voltage (LV) and the high-voltage (HV) experiments, respectively. The PIII experiments were carried out in a nitrogen plasma sustained by hot filament glow discharge. The filament rods were welded to increase the filament currents to produce more free electrons for a higher plasma density (5×10^9 ions/cm^3). The target temperature which was continuously monitored using an *in situ* thermocouple[15] during the PIII processes was kept at $300+10\,^\circ$C by varying the pulsing frequency, typically a few hundred hertz in the HV case and between 7 and 8 kHz in the LV experiments.

III. THEORETICAL SIMULATION

To determine the sheath expansion characteristics at different implantation voltages and demonstrate the advantages of the HLPIII process, theoretical simulation is conducted using a two-dimensional fluid model.[16–18] For simplicity, it can be assumed that the target is a square bar with an infinite length located on an infinite platen. The simulation parameters are chosen based on the real experimental parameters: $n_0=5.0\times10^{15}/\mathrm{m}^3$, $kT_e=1.5$ eV, and nitrogen plasma. The

[a]Author to whom correspondence should be addressed; electronic mail: paul.chu@cityu.edu.hk

 © 2000 American Institute of Physics

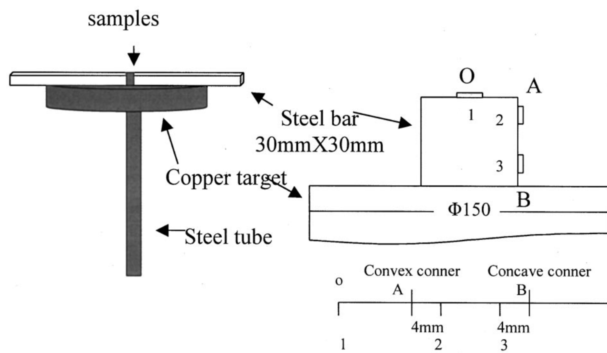

FIG. 1. Schematic of the placement of the implanted target and samples.

sheath expansion dynamics is simulated by solving the fluid model equations[16–18] by the finite difference method. Only half of the target (the right-hand side in this case) needs to be simulated on account of its symmetry. The time step is $2.78\times 10^{-4}\mu$s, and the space steps are 0.67 and 1.36 mm for 2 and 15 kV implantation voltages, respectively. The simulation ends at $\tau = 250$ (about 15 μs) considering the very slow expansion speed late in each voltage pulse.

IV. RESULTS AND DISCUSSION

Figure 2 depicts the simulated electric potential contours of the expanding plasma sheath under high-voltage (15 kV) and low-voltage (2 kV) conditions. The plasma sheath configuration at the corners is similar to the simulation results of Sheridan and Gloecker[19] and Paulus *et al.*,[20] but different on the side surface (*AB*). In this work, we simulate the more practical experimental setup in which the bar is located on a sample holder, and the plasma dynamics is influenced by the sample holder. Our results show that the expanding sheath is characterized by a smooth transition at the corner. The sheath expands faster at the concave corner and slower at the convex corner. At the concave corner, the exposed target surface per plasma volume or equivalent surface is larger and the sheath has to expand more rapidly to provide ions for implantation, and so the ion flux into these locations are different. Our results further demonstrate that the implantation voltage has a big influence on the sheath shape. The 2 kV plasma sheath is thinner (less than 2 cm), and is more conformal to the surface topography of the target.

Figure 3 displays the simulated incident dose along the top and side surfaces under high-voltage (15 kV) and low-voltage (2 kV) conditions showing different degrees of lateral nonuniformity on the exposed surfaces. As expected, the ion dose on the top surface is higher than that on the side surface in both cases. In addition, both corners receive a lower ion dose since the sheath shape and the electric field direction determine the direction of ion movement. The sheath dynamics of different implantation voltages has a critical effect on the ion flux distribution along the exposed surface. For 2 kV implantation, the target experiences a ''big target'' effect (30 mm/S_0=4.5) leading to a higher incident dose near the convex conner. The results are consistent with previous results[19–21] and are due to a surplus of ions near this corner. On the side (*AB*) surface, the incident ion dose decreases towards the lower part of the target because ions are progressively pulled to the horizontal surface. The 15 kV implantation process can be categorized to be in the ''small target'' regime relative to the sheath thickness, and so there is less ion dose variation along the top surface. The side surface also exhibits a relatively smaller variation in the ion dose. Comparing the results, it is obvious that the ion dose distribution in the low-voltage (2 kV) process is basically smooth along the exposed surface without the big change from the top surface to the side surface. This is of great importance in practical applications.

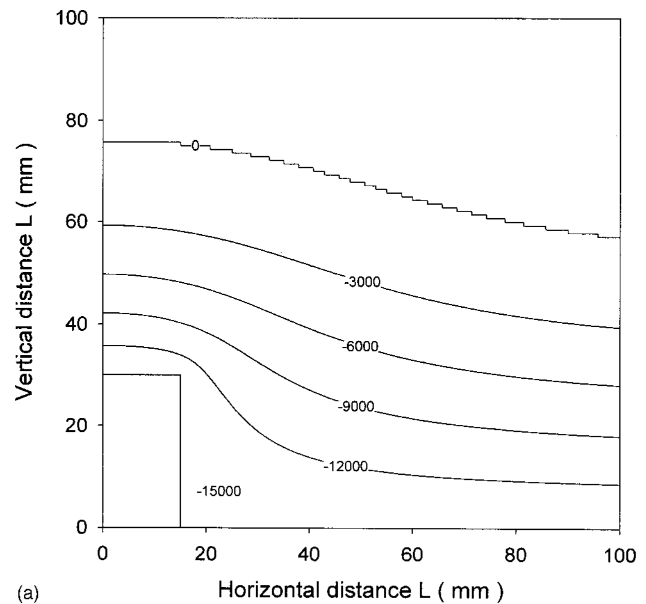

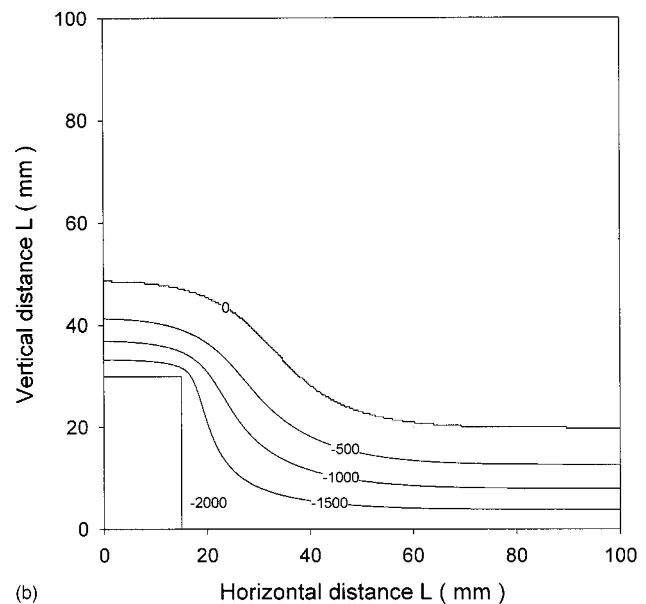

FIG. 2. Potential contours around the target at $\tau = 250$ for (a) high-voltage implantation (15 kV) and (b) low-voltage implantation (2 kV).

The ion incident angle is determined by the sheath shape as the ion movement is orthogonal to the electric potential contour displayed in Fig. 2. At the beginning of the negative pulse, the sheath is very thin and ions are implanted normal to the surface. As the sheath expands, the incident ion angle

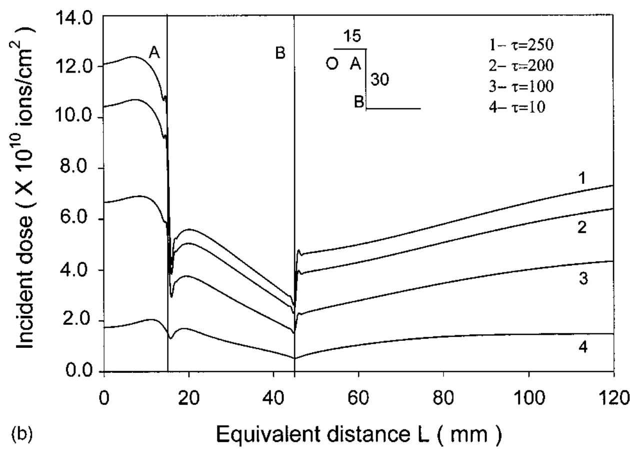

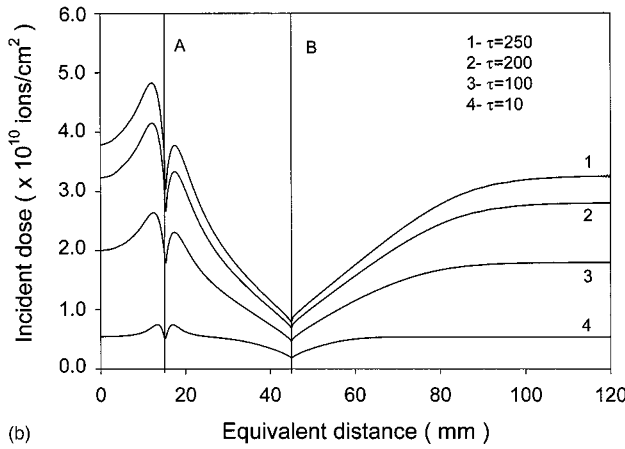

FIG. 3. Simulated incident doses on the exposed surfaces at $\tau = 250$ for (a) high-voltage implantation (15 kV) and (b) low-voltage implantation (2 kV).

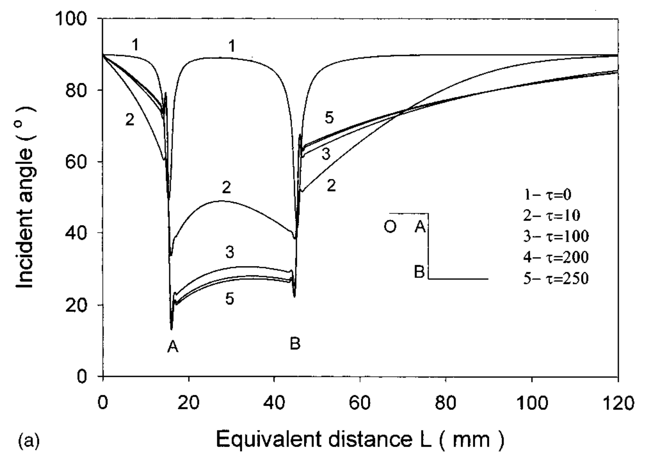

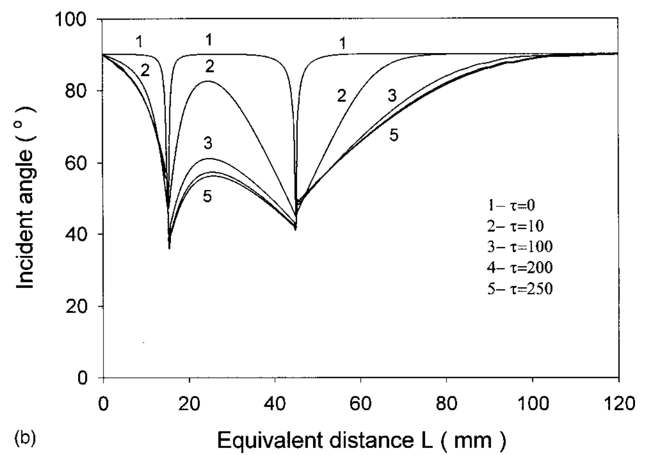

FIG. 4. Simulated incident angles on the exposed surfaces at $\tau = 250$ for (a) high-voltage implantation (15 kV) and (b) low-voltage implantation (2 kV). The incident angle is defined as the angle between target surface and the incident direction of the ions.

decreases around the corners, and the magnitude of the change depends on the voltage (Fig. 4). Comparing with the high-voltage (15 kV) case, the low-voltage (2 kV) process features a larger incident angle (less glancing) with a average angle of 50° on the side surface. However, the incident angle is lower (more glancing) on the side surface at a higher sample voltage. Sputtering is more prevalent at the glancing incidence resulting in a smaller retained dose. Therefore, it should be noted that since our simulation formalism does not take into account sputtering losses, theoretical data may not correlate with the experimental results on an absolute basis, even though the relative trends can be compared.

Figure 5 plots the ratios of the simulated total ion dose on the side surface to that on the top surface. The ratio is always less than one and varies with the implantation voltage and pulse duration. If we integrate the ion dose on the top surface and compare that to the total ion dose on the entire side surface, the dose ratio improves from 35% (high voltage) to 48% (low voltage). In field applications, only the top surface and the upper half of the side surface of a track used in a transportation mechanism are in contact with the overlying moving parts. If we compare the ion dose on half of the top surface to that on the upper half of the side surface, the dose ratio improves from 42% to 67% at $\tau = 250$. Thus, the low-voltage process gives rise to even better ion dose uniformity.

To confirm our theoretical prediction, nitrogen elemental depth profiles were determined by sputtering Auger electron spectroscopy (AES) for the three samples implanted under high- and low-voltage conditions. The results are summa-

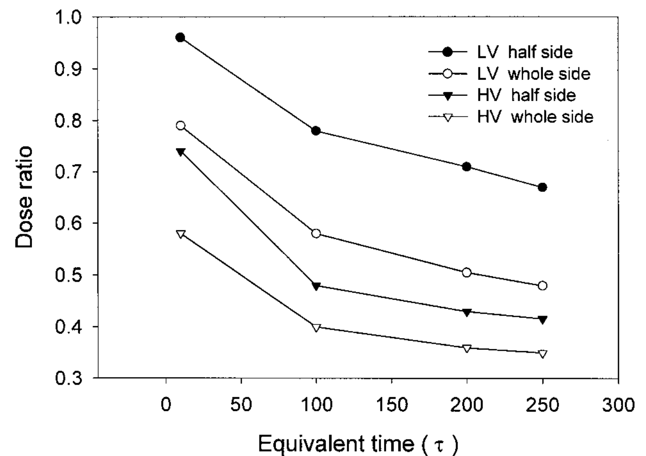

FIG. 5. Ratios of the simulated incident doses on the side surface to that on the top surface for LV and HV conditions vs equivalent time. The ion dose on the top surface is compared to that on the entire side surface or the upper half of the side (solid data point).

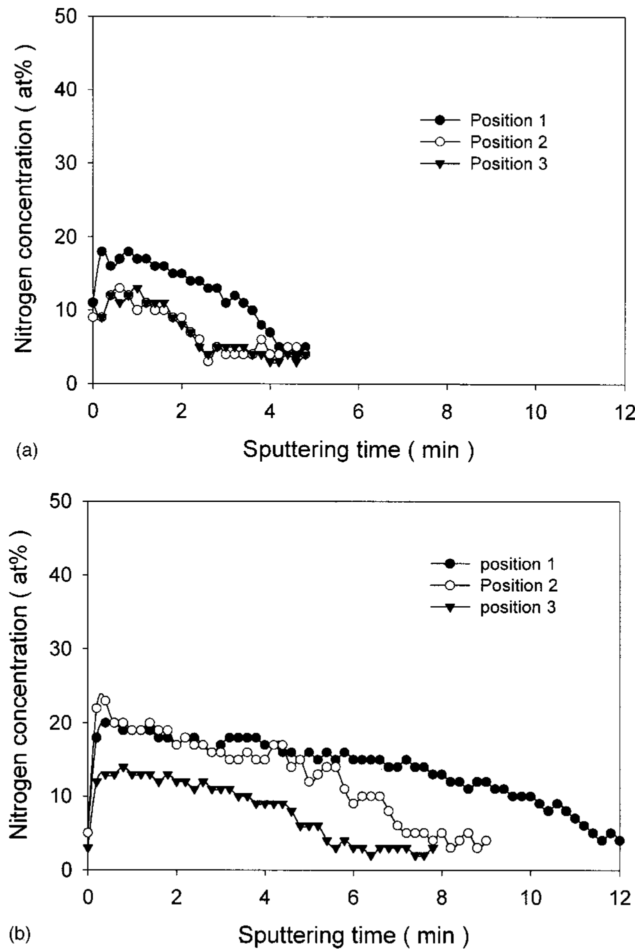

FIG. 6. AES nitrogen in-depth distributions in the three samples for (a) high-voltage implantation (15 kV) and (b) low-voltage implantation (2 kV).

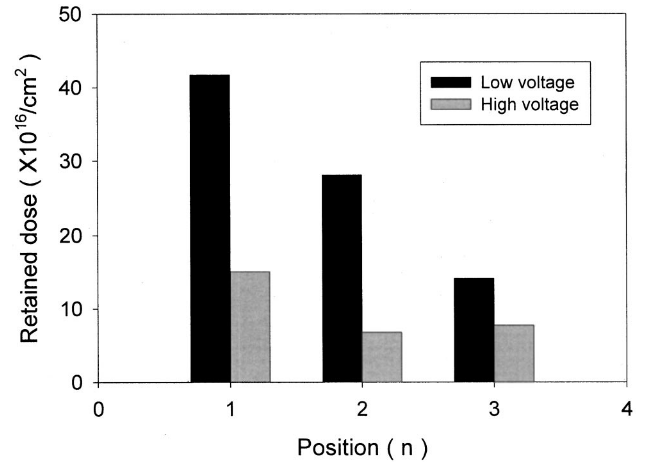

FIG. 7. Comparison of the experimental retained doses at the three different positions.

rized in Figs. 6 and 7. The same relative sensitivity factor and sputtering rates are used in the calibration of the Auger depth profiles, and in spite of minor variations of these factors throughout the profiles, relative comparison of the profiles is valid considering the big difference among the samples. Only the nitrogen profiles are shown here to facilitate comparison, but it should be noted that the surface oxygen-rich layer is thicker in the HV sample. At first glance at the retained dose distribution, the low-voltage process seemingly exhibits worse uniformity than the high-voltage sample. However, if we only consider and compare the upper part of the target (top surface and upper half of the side surface) just like a real track, the results are different. As shown in Fig. 7, the ratio of the retained dose in position 1 to that in position 2 is 1.46 for the low-voltage process. In contrast, this ratio increases to 2.22 for the high-voltage case. Our results again demonstrate the advantage of the low-voltage process in terms of retained dose uniformity.

In general, it can be observed that the experimental retained dose is qualitatively in line with the theoretical incident dose, especially for large incident angles as in the case of low-voltage implantation. It should, however, be noted that for implantation at a high glancing angle, the retained dose is affected by sputtering as indicated by our incident angle simulation. For instance, as shown in Fig. 6, the nitrogen in-depth distribution in position 2 is nearly the same as that in position 3 in the 15 kV case. Although the simulated incident dose in position 2 is higher than that in position 3, the incident angle at position 2 is smaller than that at position 3, and more sputtering takes place in position 2 leading to a lower than expected retained dose.

As shown in Fig. 6, low-voltage conditions result in a thicker modified layer. The retained doses on both the top and side surfaces are also higher under low-voltage conditions. As shown in Fig. 7, the ratios of the retained dose (low voltage to high voltage) are 2.76, 4.13, and 1.82 for positions 1, 2, and 3 , respectively. In our experiments, the sample temperature was kept constant at 300+10 °C, and so the thicker modified layer cannot be explained by a temperature effect. In order to understand the relationship between the ion dose rate and applied voltage at a constant sample temperature, we need to investigate the factors affecting the sample temperature during PIII.

The sample temperature is determined by the following factors:[22] (1) heating by the implanted ions P_1, (2) hot filament radiation heating during the glow discharge P_2, (3) collisional heating by the free particles in the vacuum, mainly the plasma P_3, (4) radiation loss P_4, and (5) heat conduction loss through the target holder P_5. In general, heating by radiation and particle collision is very small,[15] and the combined magnitude is much less than of ion heating. Hence, the sum of P_2 and P_3 can be assumed to be zero. The heat loss by conduction through the stainless steel tube connecting the sample platen to the high-voltage feedthrough P_5) can also be ignored since the tube wall is thin. After the sample temperature has achieved an equilibrium value (T),

$$P_1 = \varepsilon\sigma S(T^4 - T_0^4). \quad (1)$$

For ion heating, we can assume that $P_1 = VI_{\mathrm{ave}}$ where I_{ave} represents the average ion current and V is the applied sample voltage. Consequently,

$$I_{\mathrm{ave}} = \frac{\varepsilon\sigma S}{V}(T^4 - T_0^4). \quad (2)$$

To maintain a constant heat input and sample temperature, I_{ave} must be inversely proportional to the applied sample voltage. In our experiments, a decrease from 15 to 2 kV implies that the ion flux increases by 7.5 times in order to maintain the same treatment temperature. Hence, the sample receives a higher ion dose rate in the low-voltage process compared to the high-voltage process. We therefore postulate that the improved modified layer thickness stems from the higher average ion current density. A higher ion flux provides more nitrogen just beneath the top surface accelerating the diffusion of the incoming nitrogen, while the high voltage does not substantially contribute to the depth.

V. CONCLUSION

The implantation voltage has a large influence on the sheath dynamics including the sheath thickness, shape, ion flux, and incident angle. Our simulation results show that the thinner sheath under low-voltage conditions is more conformal to the target surface, and consequently, the incident ion flux is more uniform along the exposed surface compared to the high-voltage implantation in which the ion incident angle on the side surface is small. Our results reveal that low voltage PIII can substantially increase the modified layer thickness compared to high voltage PIII at the same treatment temperature. The thicker modified layer is postulated to be due to the higher ion current density used in the low-voltage process. In summary, the more efficient high-frequency, low-voltage plasma immersion ion implantation (HLPIII) technique is more suitable for the treatment of complex-shaped components and has a higher commercial potential. It should also be noted that HLPIII is more versatile than conventional plasma nitriding in terms of treatment voltage, plasma density, gas pressure, pulsing frequency/duration, and so on.

ACKNOWLEDGMENTS

This work was supported by the Hong Kong Research Grants Council Earmarked Grant Nos. 9040344 and 9040412 as well as the Hong Kong Research Grants Council/Germany Joint Scheme No. 9050084.

[1] J. R. Conrad, J. L. Radtke, R. A. Dodd, F. J. Worzala, and N. C. Tran, J. Appl. Phys. **2**, 4951 (1987).

[2] J. Tendys, I. J. Donnelly, M. J. Kenny, and J. T. A. Pollock, Appl. Phys. Lett. **53**, 2143 (1988).

[3] S. Mandl, N. P. Barradas, J. Brutsher, R. Guenzel, and W. Moeller, Nucl. Instrum. Methods Phys. Res. B **127/128**, 996 (1997).

[4] P. K. Chu, X. Lu, S. S. K. Iyer, and N. W. Cheung, Semicond. Sci. Technol. **40**, S9 (1997).

[5] T. Hochbauer, W. Ensinger, G. Schrag, J. Hartmann, B. Stritzker, and B. Rauschenbach, Nucl. Instrum. Methods Phys. Res. B **127/128**, 869 (1997).

[6] W. Ensinger, T. Hochbauer, and B. Rauschenbach, Surf. Coat. Technol. **103/104**, 218 (1998).

[7] M. M. Shamim, D. E. Muller, K. Sridharan, B. P. Fetherston, N. Tran, and J. R. Conrad, J. Appl. Phys. **77**, 1015 (1995).

[8] Z. M. Zeng, B. Y. Tang, P. K. Chu, X. B. Tian, S. Y. Wang, and X. F. Wang, J. Vac. Sci. Technol. B **17**, 851 (1999).

[9] A. H. Hamdi, G. W. Malaczynski, A. A. Elmoursi, C. H. Leung, A. B. Campbell, D. Shpuniarsky, S. J. Simko, M. C. Militello, M. P. Balogh, and J. H. Lindsay, J. Vac. Sci. Technol. B **17**, 828 (1999).

[10] X. B. Tian, X. F. Wang, S. Y. Wang, B. Y. Tang, and P. K. Chu, Proceedings of the Surface Engineering: Science and Technology 1, Minerals, Metals, and Materials Society (TMS) Annual Meeting, San Diego, CA, 1999, edited by A. Kumar, Y. W. Chung, J. J. Moore, and J. E. Smugeresky, p. 177.

[11] P. K. Chu and X. B. Tian, Fifth IUMRS International Conference on Advanced Materials (IUMRS-ICAM'99), Beijing, China, 13–18 June, 1999.

[12] X. B. Tian, Z. M. Zeng, B. Y. Tang, T. K. Kwok, and P. K. Chu, International Conference on Surface Modification of Metals by Ion Beams (SMMIB99), Beijing, China, 19–24 September 1999.

[13] P. K. Chu, B. Y. Tang, Y. C. Cheng, and P. K. Ko, Rev. Sci. Instrum. **68**, 1866 (1997).

[14] X. B. Tian, X. F. Wang, B. Y. Tang, P. K. Chu, P. K. Ko, and Y. C. Cheng, Rev. Sci. Instrum. **70**, 1824 (1999).

[15] X. B. Tian, Z. N. Fan, X. C. Zeng, Z. M. Zeng, B. Y. Tang, and P. K. Chu, Rev. Sci. Instrum. **70**, 2818 (1999).

[16] M. Winder, I. Alexeff, W. D. Jones, and K. E. Lonngren, Phys. Fluids **13**, 2523 (1970).

[17] M. Hong and G. A. Emmert, J. Vac. Sci. Technol. B **12**, 889 (1994).

[18] T. E. Sheridan and M. J. Alport, J. Vac. Sci. Technol. B **12**, 897 (1994).

[19] T. E. Sheridan and M. J. Gloecker, J. Appl. Phys. **81**, 7153 (1997).

[20] M. Paulus, L. Stals, U. Rude, and B. Rauschenbach, J. Appl. Phys. **85**, 761 (1999).

[21] M. Hong and G. A. Emmert, J. Appl. Phys. **78**, 6967 (1995).

[22] S. Mandl, J. Bratscher, R. Guenzel, and W. Moeller, J. Vac. Sci. Technol. B **14**, 2701 (1994).